BAYERO JOURNAL OF PHYSICS AND MATHEMATICAL SCIENCES

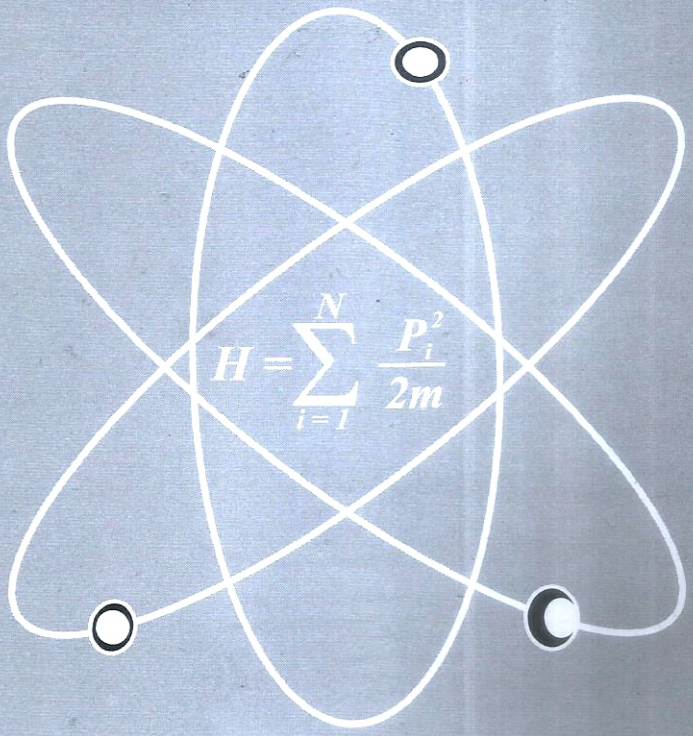

VOLUME 8, No. 1
SEPTEMBER, 2017.

Published by: THE DEPARTMENTS OF PHYSICS AND MATHEMATICAL SCIENCES, BAYERO UNIVERSITY, KANO.

MEMBERS OF THE EDITORIAL BOARD

TABLE OF CONTENTS

BAJOPMAS JOURNAL 7(1): 9 – 21
Printed in Bayero University, Kano - Nigeria.

IMPEDANCE, DIELECTRIC AND MODULUS STUDY OF Ti-doped $LiSn_2(PO_4)_3$

U. Ahmadu[1], K. U. Isah[1], A. Mann[2], M. I. Kimpa[1, 3] and S. O. Ibrahim[1]
[1]Department of Physics, Federal University of Technology, Minna.
[2]Department of Chemistry, Federal University of Technology, Minna.
[3]Department of Science, Faculty of Science, Development and Human resources, University *Tun Hussein Onn Malaysia, Batu Pahat, Jo*
Corresponding author: u.ahmadu@yahoo.com
Tel: 08066034370

ABSTRACT

$LiSn_2(PO_4)_3$ of composition $LiSn_{1.85}$ $Ti_{0.15}$ $(PO_4)_3$ with NASICON structure was prepared by solidstate synthesis. XRD results show the formation of stable phase material of rhombohedral structure with the 3c space group. Traces of unreacted SnO_2 and minor impurity of SnP_2O_7 were detected. Impedance and dielectric study in the microwave range show conductivity enhancement in bulk and grain boundary. The room temperature ionic conductivity is 4.74x10-5 S/cm and the conductivity at 740 K is 2.37x10-3 S/cm. The highest value of dielectric constant ' obtained is 2000 and the lowest value is 500. Imaginary modulus vs temperature plot indicates the presence of temperature relaxation in the material. The plot of relaxation frequency at different temperatures was used to calculate the activation energy which was found to be 0.23 eV. These imply that the material could be applied as solid electrolyte at high temperatures.

Keywords: Impedance; conductivity; dielectric permittivity; modulus; relaxation

INTRODUCTION

Solid electrolytes have many advantages over liquid electrolytes such as stability, ruggedness, miniaturization, wide range of operating temperature [1], simplicity of design, absence of leakage and pollution and better resistance to shocks and vibrations [2, 3]. In addition, solid electrolytes suffer from relatively low ionic conductivity, amongst others [4, 5].

The discovery of NASICON (Na-Super-Ionic Conductor) [6] was a major breakthrough in the tailored making of fast ion conductors (Super-Ionic Conductors) with a covalent framework structure. Apart from their potentials as solid electrolytes they find applications in conversion systems, super capacitors [7,8] sensors, displays , nuclear waste disposal, low expansion ceramics, thermal shock resistant materials and exhibit promising catalytic properties [2,9]. They have potential applications as Li ion conductors for rechargeable lithium ion batteries due their high ionic 2 conductivity, temperature stability, amongst others. Different systems such as $LiM_2(PO_4)_3$ (M=Ti, Zr, Hf, Ge and Sn) have been reported [10,11] with the Ti-based system probably the most studied due to the smaller tunnels formed with Ti4+ cations which make better fit for the lithium conductors. The Li ion conductivity of Li_1+xTi_2-x Alx $(PO_4)_3$ is up to 10-3 S/cm at room temperature. However, $LiSn_2(PO_4)_3$, an outstanding example, has been prepared via solid state reaction [12,13] with the sintering temperature reported to be very important. It is the least studied amongst members of the NASICON family [13] and has two crystallographic phases: a high temperature rhombohedral 3 symmetry phase with high ionic conductivity and a low temperature phase with triclinic *PI* symmetry, or monoclinic *Cc* symmetry with lower conductivity. Stability of the compound has been an issue [14] with teflon having been used as binder to improve the stability against breakage due to the structural transition from monoclinic to rhombohedral. But the value of the conductivity obtained was very low(10-10 S/m) at room temperature. Nevertheless, some authors [15] succeeded in obtaining stable

pellets of $LiSn_2$ $(PO_4)_3$ using mechano-chemical milling without binder and the ionic conductivity improved to 10-7 S/m at room temperature. Meanwhile, the sol-gel method has been used to overcome some of these problems due to its lower sintering temperature, shorter reaction time, good homogeneity and high specific area of the material [12, 16, 17]. Synthesis of $LiSn_2(PO_4)_3$ using low sintering temperature citric acid-assisted sol-gel method resulted in a minor phase of impurity compared with samples prepared by mechanical ball-milling. X-ray diffraction study confirmed the formation of rhombohedral phase $LiSn_2(PO_4)_3$ after sintering at 873 and 923 K for 48 h and conductivity attained at 873 K was 1.38 x 10-5 S/m, which is higher [17].

In the current work $LiSn_{1.85}$ $Ti_{0.15}$ $(PO_4)_3$ has been synthesized using solid state reaction based on a sintering regime that is expected to enhance stability and electrical conductivity in order to resolve some of the above problems. The results of TGA/DTA, X-ray diffraction, impedance spectroscopy, modulus and dielectric studies are presented to elucidate these properties.

EXPERIMENTAL PROCEDURE

$LiSn_{1.85}$ $Ti_{0.15}$ $(PO_4)_3$ was prepared by solid state reaction using agate mortar and pestle using stoichiometric amounts of analytical grade Li_2CO_3 (India > 99%), SnO_2 (99.99%), TiO_2 (BDH, 99.99%), Methanol CH_3OH (BDH, 99.99%), and NH_4H_2 PO_4 (BDH, 99.99%). Appropriate amounts of the sample were properly mixed in agate mortar and pestle along with appropriate quantity of methanol to get a homogenous semisolid paste. The homogenous paste was initially calcined at 1173 K for 4 h in order to decompose $NH_4H_2PO_4$ and initiate the reaction with the carbonate [14]. This led to the emission of carbondioxide, ammonia and water vapour. The mixture was reground to micron size and pressed into a pellet. The dimensions of the pellet was measured and inserted into a steel mould of 16.8 mm diameter by 12 mm thickness in a pelletizing machine. The powder was then pressed in a cold press for 5 min under a hydraulic pressure of 5 N/m2 with the formation of pellets of 16 mm diameter by 1.7 mm thickness. This was sintered at room temperature in alumina crucible at 1173, 1273 and 1373 K for 3 h, successively. 0.5g of sample specimen was used for thermal analysis using DTA/TGA on a TG-DTA machine (Perkin Elmer TGA 400). The data was taken from room temperature to 1113 K. XRD machine (D8 advance, Bruker AXS, 40 kV, 40 mA) with monochromatic Cu-Kα1 (λ = 1.54060Å) was used to characterise the structure and phase composition in the 2Θ range 12 to 40° and step size 0.034°. The counts were accumulated for 96 s for each step. Bragg's law ($n\lambda = 2d \sin \Theta$) was used to calculate the peak positions for diffraction experimentally, where n is an integer, λ is the wavelength of the incident X-rays, d is the inter planer spacing and Θ is the diffraction angle. The lattice parameters of the sample were calculated using equation (1).

$$\frac{1}{d^2} = \frac{4}{3}\left(\frac{h^2+hk+k^2}{a^2}\right) + \frac{l^2}{c^2} \quad (1)$$

where d is the inter planer spacing, h, k and l are Miller indices and *a* and *c* are the lattice parameters.

The crystallite size was calculated using equation (2)

$$D = \frac{k\lambda}{\beta \cos \Theta} \quad (2)$$

where D is the crystallite size, k the Scherer constant (0.94), λ the wavelength, β is the Full Width at Half Maximum (FWHM) in radians and Θ the Bragg's angle in radians.

Microstructure of surface of sample was determined by High Resolution Scanning Electron Microscope (HRSEM, Zeiss) operated at 20 kV and image captured at 5 kV. The ceramic was
positioned on an aluminium stage with the aid of carbon adhesive tape and coated with AuPd (Gold-Palladium) using a sputter coater. Impedance measurements were carried out by measurement of the complex impedance ($Z = Z' - iZ''$) and the complex electric conductivity ($\sigma = \sigma' - \sigma''$) of the samples using coaxial impedance spectrometer [18] set-up in the frequency range 300 kHz to 3 GHz. Measurements were taken every 10 K on heating the sample at 1 K per min using a fixed voltage of 200 mV in air atmosphere. The samples were covered with platinum electrode paste and heated to 1073 K. The control and acquisition of data were carried out using Origin graphing software. Temperature range of 300 to 740 K was used for all measurements.

RESULTS AND DISCUSSION

The differential thermal analysis (DTA) and the corresponding thermo-gravimetric (TG) data curves are prepared for $LiSn_{1.85}Ti_{0.15}(PO_4)_3$ from 302 to 1113 K as shown in figure 1.

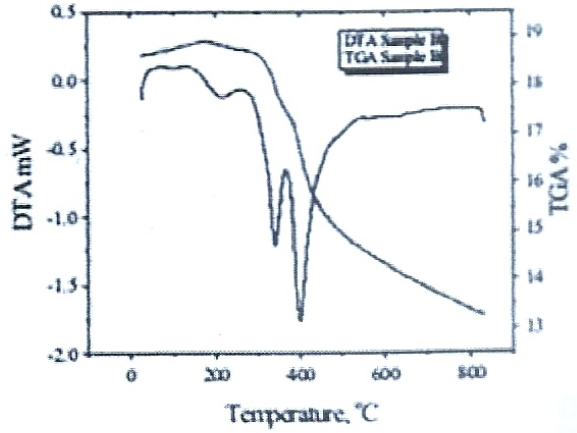

Figure 1: Simultaneous DTA-TG Plot for $LiSn_{1.85}Ti_{0.15}(PO_4)_3$ showing Exothermic and Endothermic Peaks.

NASICON precursors show a slow rate of water losses up to about 220°C. These are the first endothermic processes which are due to the evolution of water molecules. A large endothermic peak appeared at 330°C and 410°C in the DTA plot of figure 1 with exothermic peak at 370°C in between them which may be attributed to thermal effects of the decomposition of the sample precursors. The temperature 370°C is expected to be the crystallization temperature of the material. The entire thermal effect was accompanied by the evolution of various gases such as, CO_2, NH_3 and water vapour which manifests itself as single step weight loss as shown in the TG curves.

Table 1 shows the variation of density with sintering temperature for $LiSn_{1.85}Ti_{0.15}(PO_4)_3$ measured using Archimedes' principle. The unit cell volume of the sample was calculated from its structure and the lattice parameters, a *and c* were found to be 8.6122 and 21.4400 Å, respectively. The density of the sample is 3.5945 g/cm^3 (that is more than 70% of its theoretical value).

X-ray powder diffraction (XRD) analysis

XRD pattern of $LiSn_{1.85}$ $Ti_{0.15}$ $(PO_4)_3$ sintered at 11000C for 3 h is shown in figure 2. The spectrum clearly indicates the presence of rhombohedral $LiSn_2$ $(PO_4)_3$ crystalline NASICON of *R*3*c* symmetry obtained together with unreacted SnO_2 and SnP_2O_7 peaks [17]. Other authors [19] found minor phase of SnO_2 and attributed it to Li loss during high temperature sintering. The peaks around 20.9 and 21.9° 2Θ correspond to triclinic structure (phase II) and *P1*symmetry along with rhombohedral NASICON-type structure (phase I) symmetry and SnP_2O_7 [20]. The remaining peaks can be indexed in accordance with ICSD card no. 202157.

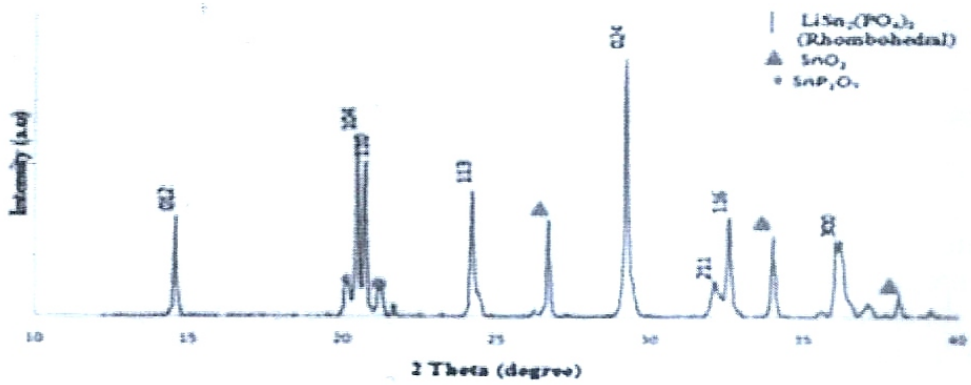

Figure 2: XRD Pattern of Sintered $LiSn_{1.85}$ $Ti_{0.15}$ $(PO_4)_3$ with Peaks of Unreacted SnO_2 and SnP_2O_7.

The lattice parameters, unit cell volume, experimental and theoretical density are presented in table 1.

Table 1: Calculated Lattice Parameters, Unit Cell Volume and Densities of $LiSn_{1.85}$ $Ti_{0.15}$ $(PO_4)_3$ Compared with Reference Sample.

Sample	a(Å)	c(Å)	V(Å)	Experimental Density (g/cm^3)	Theoretical Density (g/cm^3)	% Difference
$LiSn^{1.85}$ $Ti^{0.15}$ $(PO^4)^3$	8.5281	21.6492	1363.57	2.7568	3.5975	76.70
$LiSn^2(PO^4)^3$	8.4048	21.9621	1288.51	2.7027	3.5788	75.52

Table 1shows the lattice parameters, where the cell volume, experimental and theoretical densities of the Ti-doped $LiSn_2(PO_4)_3$ are in close agreement with literature [12] and those calculated from ICSD card no.202157. The average crystallite size was found to be 9.32μm.

SEM analysis

SEM micrograph image of $LiSn_{1.85}$ $Ti_{0,15}$ $(PO_4)_3$ for the cross-sectional surface shown in figure 3 with some agglomeration of grains of different sizes. Estimation of average grain size showed a value of 5.07μm . The sample has small grains in the μ.

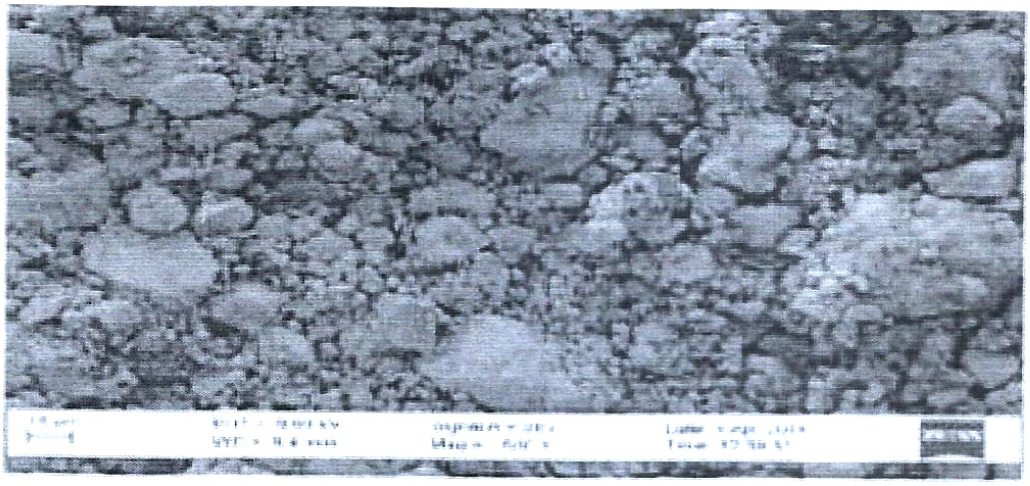

Figure 3: Microstructure of $LiSn_{1.85}$ $Ti_{0.15}$ $(PO_4)_3$ at x1000 Magnification

Complex impedance analysis

Electrode /ceramic/ electrode interface can be analysed generally by an equivalent circuit of two parallel resistance-capacitance (RC) circuit. The Nyquist plot is a complex impedance plot for the variation of real and imaginary part of impedance measured at different temperatures and is shown in figure 4(a-d) for $LiSn_{1.85}$ $Ti_{0.15}$ $(PO_4)_3$. The characteristic impedance spectrum is displayed by the appearance of the semi-circular arcs whose patterns of evolution change with rise in temperature. The shape of these plots at 300 K is almost a straight line indicating the insulating behaviour of the sample. These slopes decrease with increasing temperature up to 400 and 600 K in which the curves bend toward the real axis. With further increase in temperature to 740 K the curves become almost semi-circular (figure 4d) and are indicative of an increase in the conductivity of the sample. It is difficult to determine the values of R_g(grain resistance) and R_{gb}(grain boundary) from the complex impedance plots due to the overlap of the semicircles [21, 22]. As an alternative, the value of b (bulk conductivity) was determined by plotting imaginary part of conductivity σ "versus real part σ '. The intercepts of the dispersion curves with the -axis at high and middle frequencies give the values of b and t (total conductivity), respectively. The gb(grain boundary conductivity) is obtained by subtracting σ_b from σ_t.

Table 2: Shows the Comparison of Conductivity Values at Different Temperatures Determined from Impedance Plots for the Sample

Temp(K)	$R_b(\Omega)$	$R_{gb}(\Omega)$	b(S/cm)	gb(S/cm)	t(S/cm)
300	3.5x103	4.1x104	2.56x10-5	2.18x10-5	4.74x10-5
400	$1.50x10^3$	$3.75x10^3$	$5.98x10^{-5}$	$2.11x10^{-5}$	$8.09x10^{-5}$
600	$1.54x10^2$	$3.30x10^3$	$2.99x10^{-4}$	$2.71x10^{-5}$	$3.26x10^{-4}$
740	$4.0x10^1$	$6.80x10^2$	$2.24x10^{-3}$	$1.32x10^{-4}$	$2.37x10^{-3}$

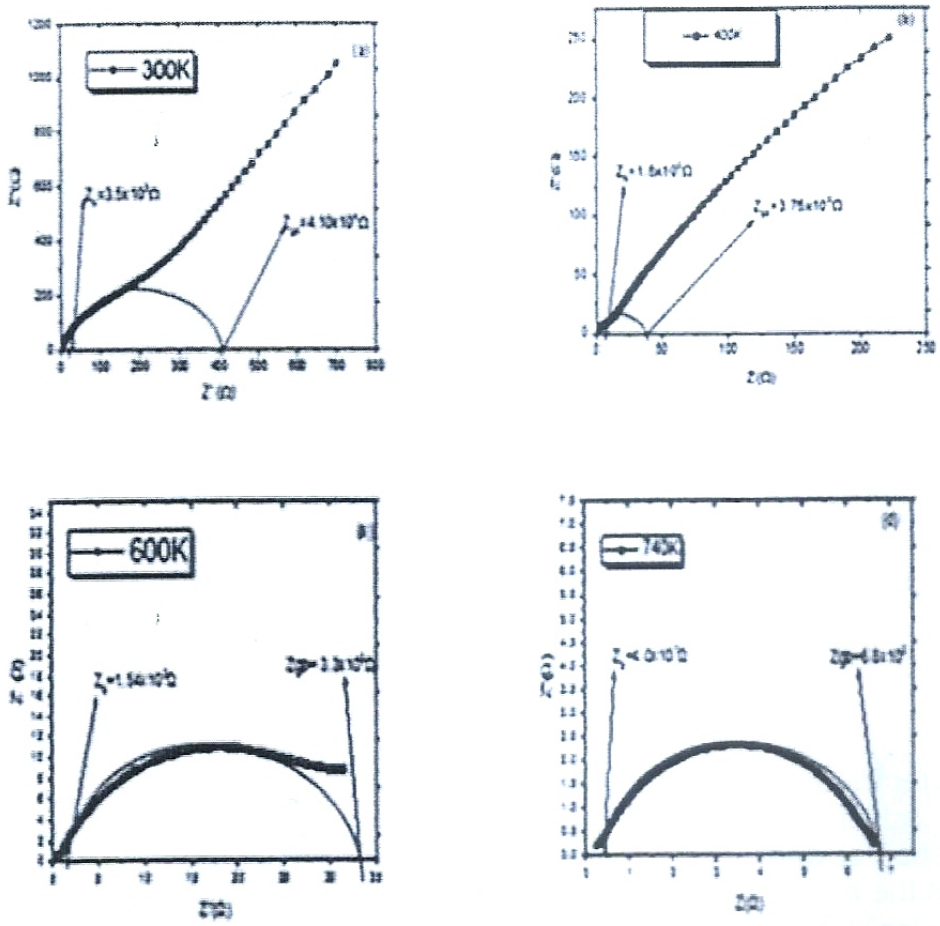

Figure 4: Impedance Plots of $LiSn_{1.85}Ti_{0.15}(PO_4)_3$ (300 to 740 K), (a) Impedance Plot of $LiSn_{1.85}Ti_{0.15}(PO_4)_3$ at Temperatures 300 (b) 400 (c) 600 (d) 740 K, showing the Extrapolations for Grain and Grain Boundaries.

Plot of real part of impedance vs frequency

Figure 5 shows the change in real part of impedance (Z') with frequency at different temperatures for Ti-doped $LiSn_2(PO_4)_3$ compound. On increasing the temperature the Z' value decreased indicating increase in ac conductivity as shown in figure 5. At higher frequencies the Z' values merge for all the temperatures due to the presence of space charge polarization [23]. The higher impedance values at lower frequencies are due to space charge polarization.

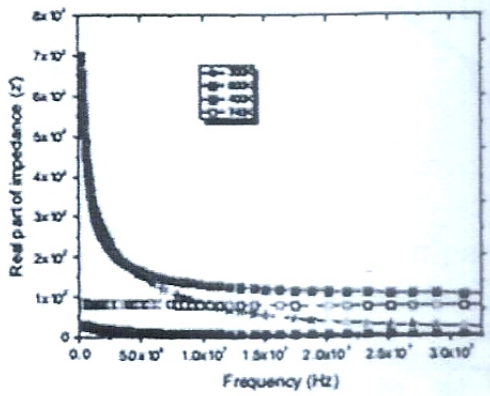

Figure 5: Variation of Real Part of Impedance with Frequency at Different Temperatures

Plot of imaginary part of impedance vs frequency

Figure 6 shows the change in real part of impedance (Z') with frequency at different temperatures for Ti-doped $LiSn_2(PO_4)_3$ compound. On increasing the temperature the Z' values decreased indicating increase in ac conductivity. At higher frequencies, Z' merge for all the temperatures due to the presence of space charge polarization [23]. The higher impedance value at lower frequencies is due to space charge polarization.

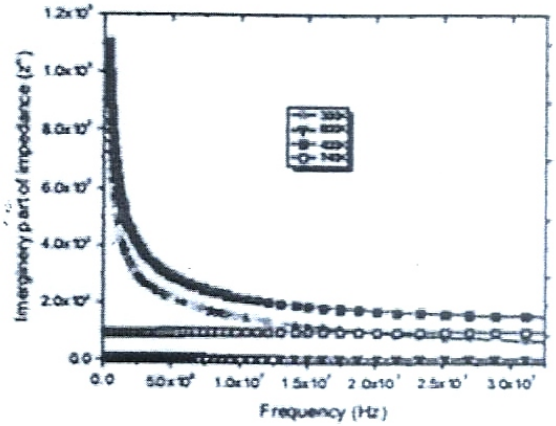

Figure 6: Imaginary Part of Impedance with Frequency

Complex electrical conductivity vs temperature

Electrical conduction in dielectric material is a thermally activated process and is due to the ordered motion of weakly bound charged particles under the influence of an electric field. It depends on the nature of the charge carriers that dominate the conduction process such as electrons/holes or cations/anions and follow the Arrhenius law. The σ_b and σ_{gb} of the compound can be evaluated from the impedance data using the relation, $\sigma_b = \frac{d}{AR_b}$, where R_b is the bulk resistance, d the thickness and A the area of the electrode deposited on the sample. R_b is obtained from the value of the low frequency intercept of the semicircle on the real axis (Z') on the complex impedance plot.

The conductivity plots shown in figure 7 consist of a semicircle and two dispersion curves at low and high σ' regions at the same time. The point of intersection of the dispersion curves with σ' axis at high frequency gives the bulk conductivity value, σ_b.

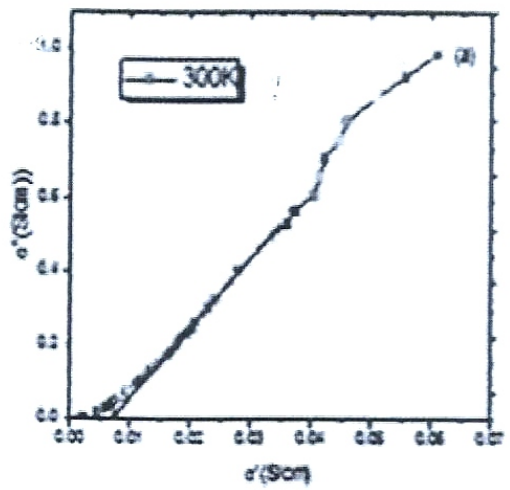

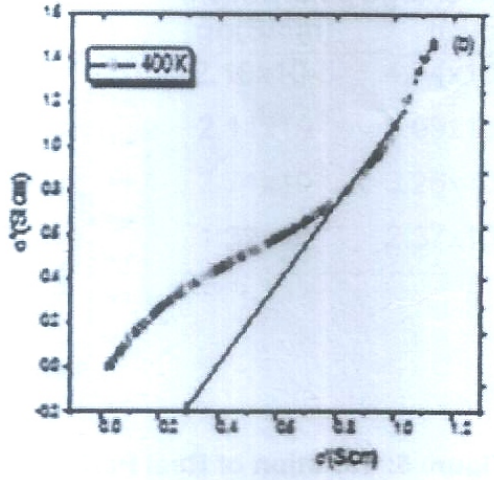

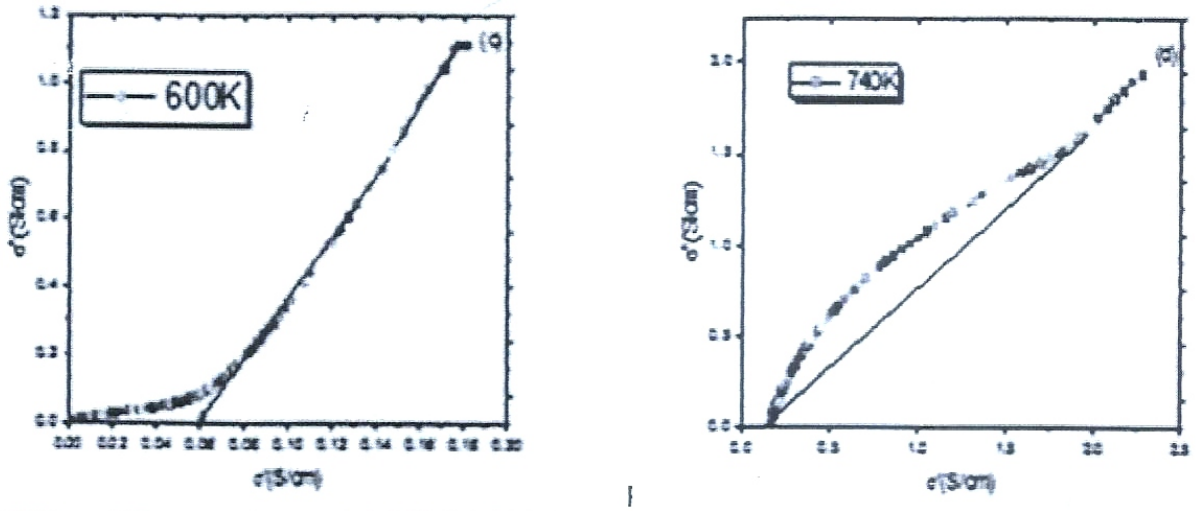

Different Temperatures: (a) 300 (b) 400 (c) 600 and (d) 740 K showing Extrapolations for Real Part of Conductivity.
The Real Part of Conductivity Increases with Temperature.

Ac conductivity vs temperature

Frequency dependent conductivity is due to the relaxation of ionic atmosphere after the movement of the particle [24]. The variation of ac conductivity as function of log of frequency at different temperatures is shown in figure 8. Jonscher explained ac conductivity using the Universal Power Law equation [25]:

$$\sigma(\omega) = \sigma(0) + A\sigma\omega^{n} \qquad (3)$$

where $\sigma(0)$ is the dc or frequency-independent part related to dc conductivity and the second term is of constant phase element (CPE) type; n is a frequency exponent in the range $0 \leq n \leq 1$. The correlation exponent n can be determined from the slope of ln ac versus lnf [26]. The ac conductivity can be calculated from equation (4).

$$\sigma_{ac} = \omega\varepsilon\varepsilon_0 \tan\delta \qquad (4)$$

The increasing trend of ac conductivity is due to the presence of disordered cations between the neighbouring sites and the presence of space charges that vanish at higher temperatures and frequencies. The change in slope takes place at a particular frequency known as the *hopping frequency* ω_p and obeys the relation [27]:

$$\sigma(\omega) = K\omega_p\left[1 + \left(\frac{\omega}{\omega p}\right)\right]^{n}, \qquad (5)$$

where all terms have been defined as usual.

Dielectric vs Temperature and Frequency

Figure 8 shows the plot of imaginary part of dielectric permittivity ϵ'' versus real part of dielectric permittivity ϵ' which increases with temperature. The value of the imaginary part of dielectric permittivity is very high (2000) while that of real part of dielectric constant is very low (340) due to the effect of space charge polarization and/or motion of conducting ions [23].

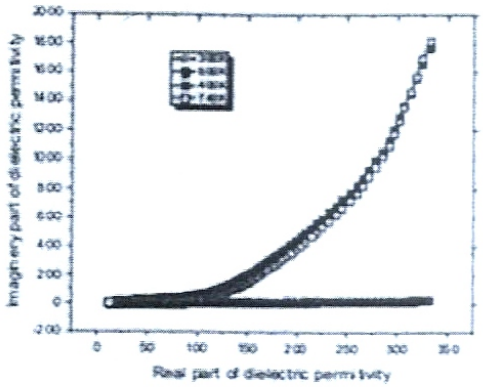

Figure 8. Plot of Dielectric Constant ε′ Versus Dielectric Loss (ε″) of Ti-doped $LiSn_2(PO_4)$ at Different Temperature (300 to 740 K).

To acquire more information on the dynamic properties of the ion in the material, the frequency dependence of the dielectric constant ′ and dielectric loss ϵ" for the $LiSn_{1.85}$ $Ti_{0.15}$ $(PO_4)_3$ at different temperatures are depicted in figures 9 and 10.

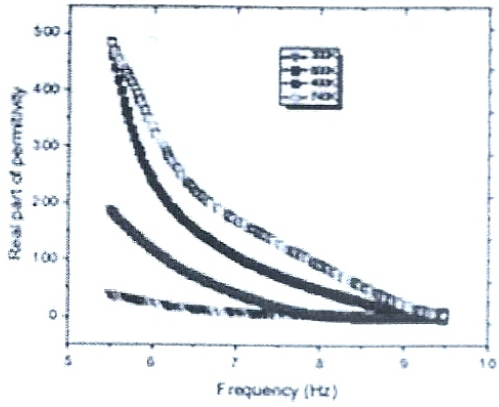

Figure 9: Plot of Relative Dielectric Constant (ε′) of Ti-doped $LiSn_2(PO_4)_3$ as a Function of log f at Different Temperatures

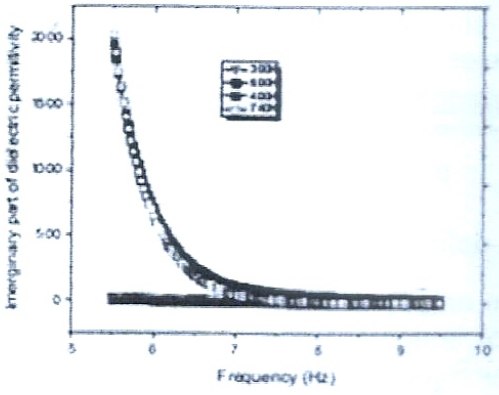

Figure 10: Plot of dielectric constant (") of Ti-doped LiSn2(PO4)3 as a Function of log f at Different Temperatures.

At low frequencies the high value of dielectric constant (ε′ ~ 500) is due to the contribution of charge carrier accumulation at the interface of electrode and the $LiSn_2(PO_4)_3$ material.

Also at high frequencies the dielectric constant ε′ and dielectric loss ε" decrease to a constant value. Meanwhile, the values of dielectric loss are very high (ε" ~ 2000) at these frequencies because the electrical energy loss is high because some of their energy is lost to the lattice as heat due to ion motion. At high frequencies the values of dielectric constant ε′ and dielectric loss ε″ are low and decrease to a constant value due to high periodic reversal of the field and to limitations of dielectric loss sources (ion vibration only), respectively [28].The ε′ and ε" values increase with increase in temperature indicating that bound charge carriers get sufficient excitation energy to be able to follow the charge in external field more easily. This in turn increases their contribution to polarization resulting in increase in ε′ and ε″ [29].

Tanδ vs Frequency Plot at Various Temperatures.

Figure 11 is the plot of frequency dependence of tan δ(loss tangent) at different temperatures and indicates a peaking behaviour for some temperatures. As the temperature increases, the tan δ peaks are shifted toward higher frequencies. The peaks are expected when the hopping frequency of ions is approximately equal to the external applied electric field. In this, case $\omega\tau = 1$, where τ is the relaxation time of the hopping process and is the angular frequency of the external field ($\omega = 2\pi f_{max}$).

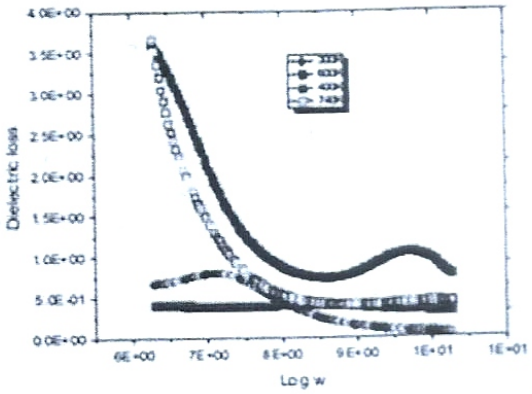

Figure 11: The Plot of Frequency Dependence of tan vs log w at Different Temperatures

The frequency dependence of imaginary part of modulus M'' at different temperatures has been plotted (figure 12) in order to determine the relaxation frequencies. The imaginary part of electric M'' modulus is indicative of energy loss under electric field [11], while M'' rises smoothly to a peak value, and two of the peaks decrease at high frequency [11]. The low frequency side of the peaks is an indication of long range motion in which the ions drift to a long distance and the position of the peaks can be attributed to a transition from short range to long range mobility as the frequency decreases [11].The shifts in M'' maxima indicate the presence of temperature relaxation process in the material [11]. When the conductivity plots of frequency are analysed, the shifts in frequency of the M'' peaks correspond to conductivity relaxation phenomenon [30]. The real part of electric modulus (M'), on the other hand, represents the ability of a material to store energy and increases with increase in temperature at low frequencies (figure 13). The maxima of M' falls with increase in temperature in all the plots and M' tends to lower values, confirming that electrode effects make negligible contribution and may be ignored in the modulus at low frequencies and temperatures [11]. The frequency independent variation of at high frequencies may be attributed to absence of charge effects due to inhomogeneities in composition.

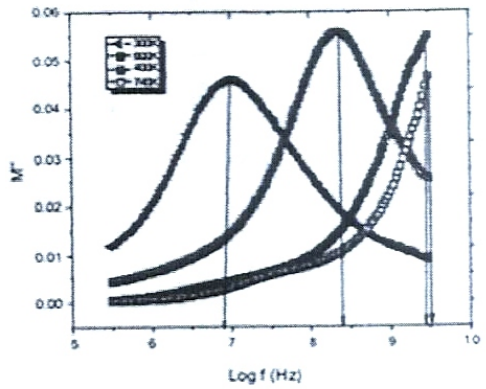

Figure 12: Plot of Frequency Dependence on at Different Temperatures Indicate the Relaxation process

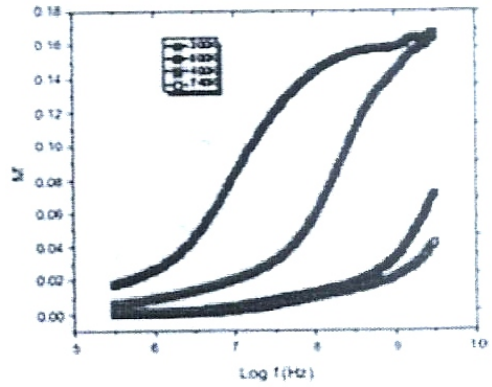

Figure 13. Plot of Real Part of Electric Modulus (M'') Versus Frequency at Different Temperatures

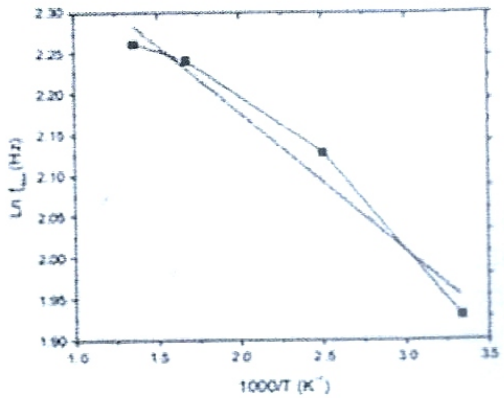

Figure 14. Plot of the Peaks of in $M''(f_{max})$ vs 1000/T

The values of the peaks of M'' **(i.e. f_{max})** are plotted in figure 14 against 1000/T. The peaks are expected when the hopping frequency of the ions is approximately equal to the external applied electric field. In the case $\omega\tau = 1$, where τ is the relaxation time of hopping process, ω the angular frequency of the external field $\left(\omega = 2\pi f_{\max}\right)$, $\tau = \sigma_b = \frac{1}{\omega}$. The natural logarithm of the relaxation frequencies at different temperatures have been plotted against reciprocal temperature. It was fitted to the Arrhenius equation of the form $2\Pi f_{\max} = f_o exp\left(\frac{-Ea}{KT}\right)$, where f_o is the pre-exponential factor, the activation energy for

relaxation, k the Boltzmann constant and T is the absolute temperature. From slope the value of E_a~ 0.23eV.

CONCLUSION

Powdered $LiSn_{1.85}$ $Ti_{0.15}$ $(PO_4)_3$ has been prepared by conventional solid-state reaction. XRD patterns of calcined sample showed the formation of rhombohedral symmetry with space group *R*3*c* and unreacted SnO_2 phase coexisting with triclinic SnP_2O_7. Analysis shows decrease in lattice parameter *c;* while *a*, the unit cell volume (V) and the densities (both experimental and theoretical) increased compared with reference (pristine). The experimental density is ~3.6 g/cm3(~77% of theoretical density). The crystallite size and the particle size of the sample decreased comparatively. Electrical conductivity studies show conductivity of order of 4.74x10-5 S/cm at room temperature, that is, two orders of magnitude higher than those reported in literature. The highest conductivity achieved was 2.37x10-3 S/cm at 740 K. The results indicate that the sintering temperature was instrumental in the enhancement in electrical conductivity and thus makes the sample applicable as solid electrolyte at high temperatures.

ACKNOWLEDGEMENTS

This work was supported by the Tertiary Education Trustfund (TETFUND) under project no: TETFUND/ FUTMINNA/2014/04. One of the authors, U. Ahmadu is grateful to Professor Tomas Alkus, Vilnius University, Lithuania for help with Broadband impedance and dielectric spectroscopy characterisation.

REFERENCES

[1] Fusco, F. A., Tuller, H. L., Laskar, A. L., & Chandra, S. (1989) (Education.), Super Ionic solids and solid electrolytes. Recent Trends academic press, New York), P. 43.

[2] Thangadurai, V. & Weppner, W. (2006). Recent progress in solid oxide and lithium ion conducting electrolytes research', *Solid state Ionics*, 12, 81–92.

[3] Knauth, P. (2009). Inorganic solid Li ion conductors: An overview, *Solid State Ionics,* 180, 911-916.

[4] Brodd, R. J., Huang, W., & Akridge, J. R. (2000). Macromolecular Symposia, Polymer battery R&D in the U.S, 159, 229–245.

[5] Kanno, R., & Murayama, M.(2001). Lithium ionic conductor thio-LISICON: The Li2S-GeS2-P2S5 system. *Journal of Electrochemical Society*, *148*, A742–A746.

[6] Hong, H. Y. P. (1976). Crystal structures and crystal chemical in the system Na1+xZr2SixP3-xO12. *Material Research Bulletin,* 11, 173–182.

[7] Sekido, S. & Ninimoya, Y.(1981). Fast Ionic Conductors and Their Theoretical models. *Solid State Ionics*, 34, 15315.

[8] Pham-Thi, M., Velasco, G. & Colomban, P. H.,(1986). *Journal of Material Science. Letter,* 5, 415.

[9] Yamamoto, K. and Abe, Y. (1998). Bioactive material and processing. *Journal of thermal spray technology* 81, 2201.

[10] Ahmadu, U.(2014). NASICON: Synthesis, Structure and Electrical Characterisation, in *Advanced Sensor and Detection Materials.* eds., A. Tiwari and Mustafa M. Demir, WILEYScrivener publishing, U.S.A.pp.265-300.

[11] Ahmadu, U., Salkus, T., Abubakar, O. M. and Kasim, U.I.(2011). Electrical and dielectric characterization of Na0.5Li0.5Zr2(PO4)3. *Open journal of physical chemistry*, 1, 94-103.

[12] Norhaniza, R., Subban, R. H. Y. and Mohamed, N. S. (2010). "Effecting of sintering Temperature on the Structure and Conductivity of $LiSn_2(PO_4)_3$ Prepared by Mechanical Milling Method". *Advanced Materials Research*, 338, 129-131.

[13] Cui, W. J., Yi, J., Chen, L, Wang, C. X., & Xia,Y. Y. (2012). Synthesis and Electrochemical Characteristics of NASICON Structured $LiSn_2(PO_4)_3$ Anode Material for Lithium-ion Batteries. *Journal of Power Sources* 217,77.

[14] Lazarraga, M.G., Iban˜ez, J., Tabellout, M., & Rojo, J. M. (2004). On the Aggregation Process of Ceramic LiSn2P3O12 Particles Embedded in Teflon Matrix . *Compose Science Technology,* 64, 759

[15] Norhaniza, R., Subban, R. H. Y., & Mohamed, N. S. (2013). Cr and V Substituted LiSn2P3O12. *Journal of Power Sources,* 244, 300-305.

[16] Adnan, S. B. R., & Mohamed, N. S. (2014). Properties of Novel Li4−3xCrxSiO4 Ceramic Electrolyte. *Ceramic International,* 40, 5033.

[17] Mustaffa, N. A., & Mohamed, N. S. (2015). Properties of Stannum-Based Li NASICONStructured Solid Electrolytes for Potential Application in Electrochemical Devices. *International Journal of. Electrochemical Science,*.10, 5382 – 5394

[18] Kezionis, A., Kazakevicius, E., Salkus, T., Orliukas, A. (2011). Broadband High Frequency Impedance Spectrometer with Working Temperatures up to 1200 K. *Solid State Ionics*, 188, 10 -113.

[19] Catti, M., Stramare, S., Ibberson, R. (1999). Lithium Location in NASICON-type Li+ Conductors by Neutron Diffraction. Triclinic Alpha LiZr2(PO4)3, *Solid State Ionics,* 123, 173–180.

[20] Martinez-juarez, A., Rojo, J. M, Iglesias, J. E., & Sanz, J. (1995). Reversible Monoclinicrhombohedral Transformation in LiSn2(PO4)3 with NASICON-type Structure. *Chemical Matter,* 7, 1857.

[21] Orliukas, A. F,,Dindune, A, Kanepe,. Z, Ronis, J., Bagdonas., B., & Kezionis, A. (2006).*Electrochemical Acta*, 51, 6194.

[22] Sobiestianskas, R., Dindune, A., Kanepe, Z., Ronis, J., Kezionis, A.,Kazakev, E., & Orliukas, A. (2000). *Material Science Engineering B*, 76, 184-533.

[23] Suchanicz, J. (1998). 'The Low Frequency Dielectric Relaxation Na0.5Bi0.5TiO3 Ceramic". *Material Science and Engineering*, 55, 114-118.

[24] Jonscher, A. K. (1977). The Universal Dielectric Response. *Nature,* 276, 673–679.

[25] Vijayakumar, M., Hirankumar, G., Bhuvaneswari, M. S, Selvasekarapandian, S. (2003). Influence of B2O3 Doping on Conductivity of LiTiO2 Electrode Material. *Journal of Power Sources*, 117, 43.

[26] Ahmadu, U., Tomas, S., Jonah, S. A., Musa, A. O., & Rabiu, N. (2013). Equivalent Circuit Models and Analysis of Impedance Spectra of Solid Electrolyte Na0.25Li0.75Zr2(PO4)3, *Advanced Materials Letters,* 4(3), 185-195.

[27] Almond, D. P., Duncan, G. K., & West, A. R. (1983). Anomalous Prefators in Fast ion Conductors – Nature. *Solid State Ionics,* 8, 159-164.

[28] Hegab, N. A., Bekheet, A. E, Afifi, M. A., Wahaba L. A., & Shehata, .H. A.(2007). Effect of Cd Addition on the AC conductivity and dielectric properties of Ge 70 Te films *Journal of electronic Resources*, 30, 3- 71.

[29] El-Metwally, E. G., Fadel, M., Shakra, A.M. &.Afifi, J. (2008) Optoelectronics and Advanced Materials, 10, 1320.

[30] Venkateswara Rao, A., Veeraiah, A., Prasada Rao, V.,Kishore Babu, B., & Brahmayya, M. (2014). Spectroscopic Characterization and Conductivity of Sn-substituted LiTi2(PO4)3. *Resources on Chemical Intermediate*, 40, 2.